Single Non-Noble Metal Atom Doped C_2N Catalyst for Chemoselective Hydrogenation of 3-Nitrostyrene

Huaquan Huang, ChangpingJian, Yijia Zhu, Rou Guo, Xujian Chen, Fang-Fang

Wang,* De-Li Chen,* Fumin Zhang, Weidong Zhu

Key Laboratory of the Ministry of Education for Advanced Catalysis Materials,

Institute of Physical Chemistry, Zhejiang Normal University, 321004 Jinhua, China

Corresponding Author:

Fang-Fang Wang: wangff@zjnu.cn

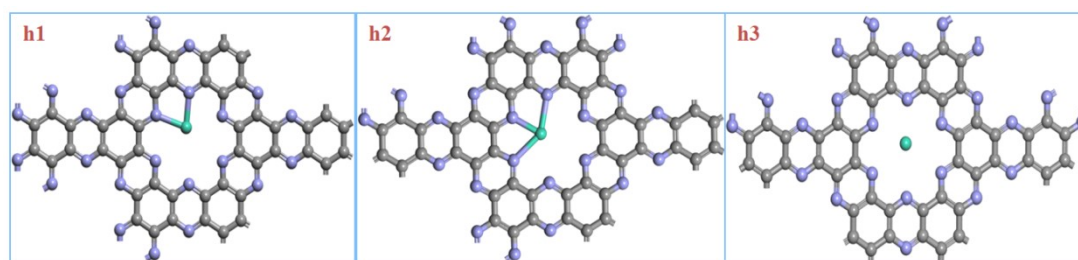De-Li Chen: chendl@zjnu.cn

1. Stable configurations of M-C$_2$N

Figure S1. Three different binding sites for metal atom embedded in C$_2$N.

For a series of single metal atoms, their optimal adsorption sites on the C$_2$N are different. As shown in Figure S1, the optimal adsorption sites can be categorized into three groups. Due to the different atomic radii, the metal atom can bind to two nitrogen atoms, three nitrogen atoms, or locate at the center of the hole, respectively, labeled as h1, h2, and h3. The previous report[1] shows that the structures with metal atom at the h1 and h2 sites are almost isoenergetic for most of the metal atoms, and only a few metal atoms are stable at site h3. The optimized structures for the stable M-C$_2$N catalysts are shown in Figure S2. The binding energy of metal atom in the C$_2$N, the charge transfer between the metal and the C$_2$N, and the magnetic moment of M-C$_2$N are listed in Table S1. It is necessary to note that the optimal magnetic moment for M-C$_2$N is obtained by setting different initial magnetic moment, and the optimal magnetic moment is obtained for the structure with lowest energy. Take the Mn-C$_2$N for example, the optimal magnetic moment for Mn-C$_2$N is 4.24 μB, while the Mn-C$_2$N with magnetic moments of 1.00, 3.00, 5.00 μB are higher in energy by 1.09, 0.03, and 0.02 eV, respectively. It is noted that the full relaxation of Mn-C$_2$N with different initial magnetic moments tends to find its optimal magnetic moment (4.24 μB) for Mn-C$_2$N. The binding energy of metal atom in M-C$_2$N is defined as $E_{binding} = E(C_2N) + E(M) - E(total)$ with the reference energy of C$_2$N sheet and isolated M atom. To evaluate the deformation of the C$_2$N due to the bonding between the transition metal and C$_2$N sheet, the deformation energy (E_{def}, positive value) was estimated by calculating the energy difference between the optimized C$_2$N sheet and the frozen C$_2$N configuration from the M-C$_2$N structure (without optimization). Then, the constrained bonding energy between the metal and C$_2$N sheet was calculated by subtracting the E_{def} from the $E_{binding}$, measuring the direct interaction between distorted C$_2$N and metal atom. As shown in Figure S3, the deformation energy is smaller than 1.05 eV for all of the

20 metals, and thus the evolution of the constrained bonding energy for M-C$_2$N is similar to that of
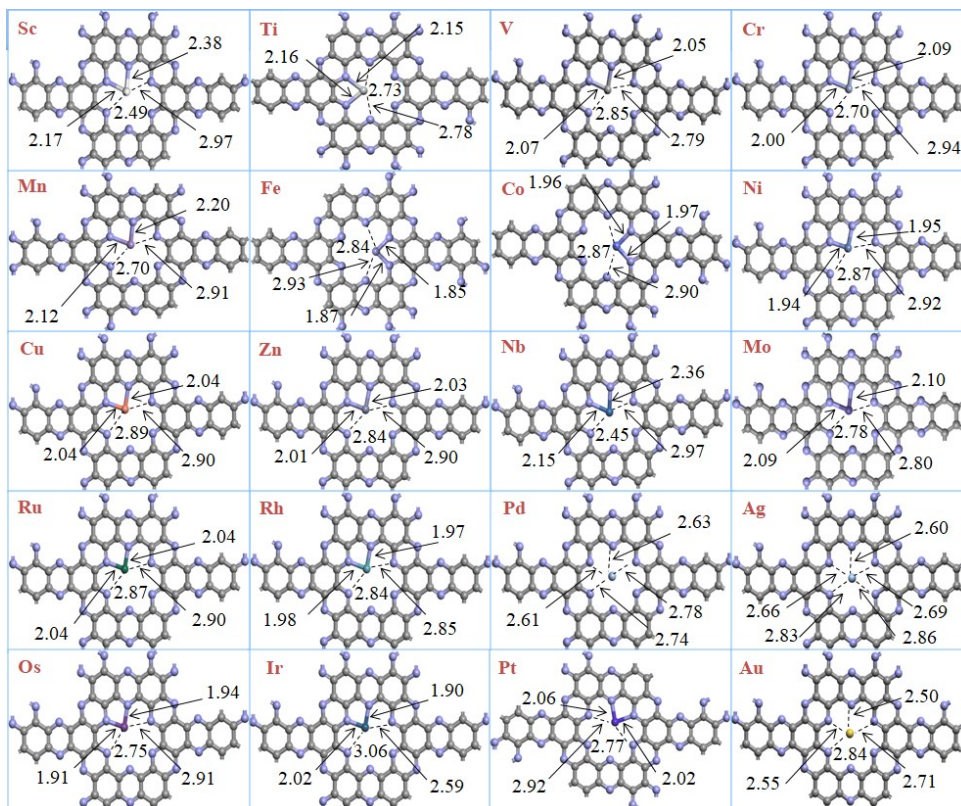
binding energy as shown in Figure 1a.

Figure S2. Stable configurations for a series of M-C$_2$N with bond lengths in unit of Å.

Table S1. Calculated binding energy of metal atom incorporated in C$_2$N, magnetic moment of M-C$_2$N, as well as Bader charge of M atom

M-C$_2$N	$E_{binding}$	Magnetic moment (μB)	q_M (|e|)
Sc	6.98	0.00	1.69
Ti	6.33	1.97	1.61
V	5.39	3.09	1.42
Cr	3.86	3.12	1.27
Mn	3.82	4.12	1.23
Fe	4.57	3.56	1.02
Co	4.97	1.59	0.88
Ni	4.00	1.36	0.78
Cu	2.69	0.00	0.74
Zn	0.82	0.00	1.16
Nb	7.71	1.59	1.52
Mo	7.07	2.49	1.22
Ru	5.43	0.57	0.77
Rh	4.40	0.00	0.64

Pd	2.60	1.22	0.64
Ag	2.23	0.00	0.65
Os	1.95	0.05	0.76
Ir	5.47	0.00	0.65
Pt	3.45	0.75	0.57
Au	1.49	0.00	0.65

The cohesive energy for Mn bulk is 2.92 eV, smaller than the absolute value of 4.31 eV for the binding energy of Mn confined in C_2N, indicating that the Mn atom is more favorable to be doped in C_2N than the aggregation into bulk. Also, the binding energy per Mn atom in Mn_2-C_2N was calculated to be -3.49 eV, weaker than that for Mn-C_2N, suggesting that the Mn atom is thermodynamically more favorable to be dispersed in the holes of C_2N. The stability of the single metal Mn-C_2N was further confirmed by calculating the migration energy of Mn atom. Two paths were considered, one is from the site with the lowest energy (in the hole) to the top of the C_6 ring and the other is from the hole to the top of the N_2C_4 ring, which are denoted as path 1 and 2, respectively, as shown in Figure S4. The migration energy for Mn atom were calculated to be 4.42 and 3.77 eV, for path 1 and 2, respectively, which are too high to be overcome, suggesting that the single Mn atom anchored Mn-C_2N is very stable. The AIMD simulations were also performed for Mn-C_2N with NVT ensemble at temperature of 373 K and time step of 1 fs. During the total simulation time of 5 ps, the Mn atom is stably located in the hole of C_2N sheet, indicating the catalyst is stable. Therefore, it is possible to synthesize Mn-C_2N material when the amount of Mn precursor is carefully controlled during the synthesis.
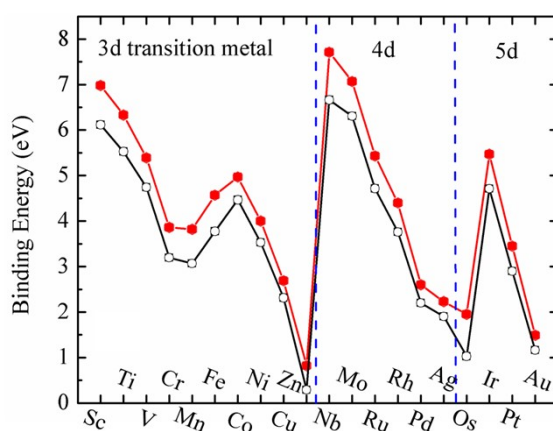

Figure S3. Binding energy of transition metal embedded in C_2N sheet (filled red circle) and constrained bonding energy between transition metal and C_2N (empty black circle).
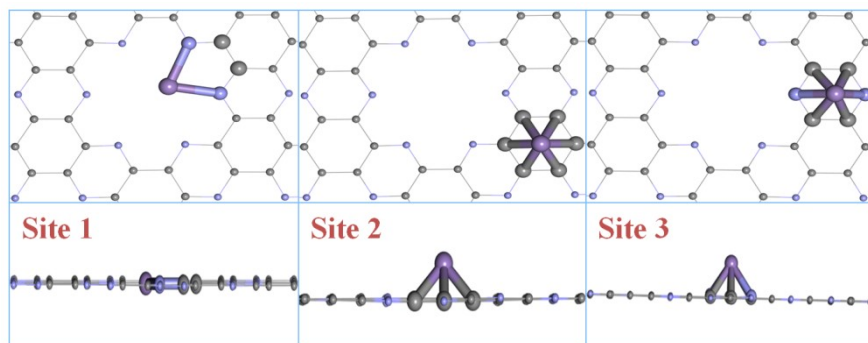
Figure S4. The structures of the different sites along the path for Mn diffusion.

2. Adsorption energies of 3-nitrostyrene on M-C$_2$N

   Many different structures were considered as starting configurations to search for the stable structures of 3-nitrostyrene molecule on M-C$_2$N with different adsorption modes. The adsorption energies for the most stable structures with different modes are given in Table S2. The optimized structures for the adsorption of 3-nitrostyrene on Mn-C$_2$N with different adsorption modes are shown in Figure S5.

   As discussed in the manuscript, there is a trend for the adsorption affinity of nitro adsorption mode, and the Sc-C$_2$N has the strongest adsorption affinity among the 3d M-C$_2$N. As shown in Table S2, the adsorption energy for the C=C adsorption mode is -0.86 and -0.96 eV for Sc-C$_2$N and Ti-C$_2$N, respectively, and then gradually decreases to 0.02 eV for Mn-C$_2$N, indicating that the C=C adsorption mode is also less favorable as the 3d electrons increases up to 3d^5. However, the Fe-C$_2$N has the largest adsorption energy of -1.67 eV and then further decreases as the electronic state from 3d^6 to 3d^{10}. Overall, the highly spin-polarized Mn-C$_2$N materials is relatively unfavorable for the adsorption of both C=C and nitro groups. For the 4d non-noble M-C$_2$N, the C=C adsorption mode has large adsorption energy, $e.g.$, the Nb-C$_2$N has a large value of -1.86 eV, much stronger than the value of -0.58 eV for V-C$_2$N in the same Group 5. Similarly, the value of -1.09 eV for Mo-C$_2$N is also larger than the value of -0.27 eV for Cr (Group 6) embedded C$_2$N. The much larger adsorption energy of the C=C adsorption explains why they are not suitable for the selective adsorption of nitro group. For all of the noble-metal (Group 8 and 9), the π-bonding between C=C and d electrons of metal is relative stronger than the interaction between the d electrons and nitro group, thus the nitro group is less favorable.

Table S2. The adsorption energies (eV) for 3-nitrostyrene on M-C_2N with different adsorption modes

M-C_2N	E_{ads}(phenyl)	E_{ads}(C=C)	E_{ads}(nitro)
Sc	-0.63	-0.86	-1.55
Ti	-0.59	-0.96	-1.30
V	-0.35	-0.58	-0.92
Cr	-0.16	-0.27	-0.65
Mn	0.25	0.02	-0.32
Fe	-1.29	-1.67	-0.76
Co	-0.57	-0.90	-0.77
Ni	-0.31	-0.60	-0.40
Cu	-0.42	-0.73	-0.49
Zn	-0.20	-0.46	-0.89
Nb	-1.07	-1.86	-1.60
Mo	-0.44	-1.09	-0.67
Ru	-0.62	-1.17	-0.44
Rh	-0.10	-0.40	-0.09
Pd	0.00	-0.37	0.14
Ag	-0.02	-0.10	-0.09
Os	-0.74	-1.38	-0.64
Ir	-0.20	-0.63	-0.03
Pt	0.01	-0.74	-0.06
Au	-0.25	-1.21	-0.05

3. Screening of the catalysts

Among the six M-C$_2$N candidates with selective adsorption of nitro group, the binding energy of Zn in C$_2$N sheet is only 0.82 eV, even smaller than the cohesive energy of 1.35 eV, suggesting that it is unstable and thus not considered as candidate. To screen the potential catalysts for the hydrogenation of 3-nitrostyrene, the rate-determining step (H transfer from metal site to N site) was computed for Sc-C$_2$N, Ti-C$_2$N, V-C$_2$N, and Cr-C$_2$N, with barriers of 0.59, 1.00, 0.95, and 0.86 eV, respectively. Therefore, the energy barriers for Ti-C$_2$N, V-C$_2$N, and Cr-C$_2$N are larger than 0.71 eV for Mn-C$_2$N. The present data cannot exclude the potential application of Sc-C$_2$N. Considering the Mn is the 3rd most abundant transition metal, the Mn-C$_2$N was adopted as the catalyst model for studying the hydrogenation of 3-nitrostyrene.
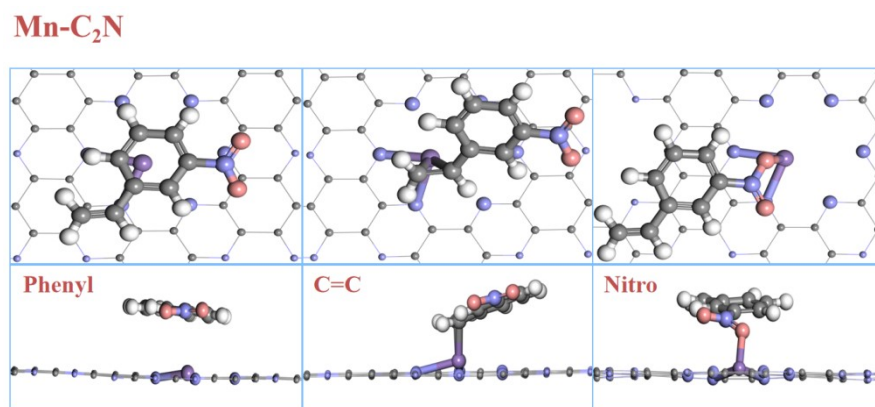
Mn-C$_2$N

Figure S5. The representative structures with different adsorption modes (phenyl, C=C, nitro) for 3-nitrostyrene adsorption on Mn-C$_2$N.

4. Comparison of the H$_2$ dissociation with PBE and PBE-D3 methods

The comparison of the adsorption and dissociation processes of H$_2$ molecule on Mn-C$_2$N is given in Figure S6. With the inclusion of dispersion force, the adsorption energy of H$_2$ molecule on Mn-C$_2$N is slightly stronger, from –0.17 (PBE) eV to –0.24 (PBE-D3) eV. The PBE-D3 calculated dissociation energy of 0.13 eV is slightly lower than 0.17 eV (PBE), and the diffusion energies for H(Mn) to N3 site are both 0.86 eV for PBE and PBE-D3 methods. Therefore, the inclusion of dispersion to PBE method only slightly changes the energy barriers, while the reaction processes are the same. In addition, the rate-determining step for the complete reaction pathways was also computed using PBE-D3 method, and the computed value of 0.59 eV is also similar to that (0.71 eV) based on PBE method. This comparison suggests that the PBE method is

reliable to compute the reaction pathways and the obtained energy barriers are reasonable. In addition, the k-point mesh of 2×2×1 was also compared to 3×3×1. For example, the adsorption of H_2 molecule on Mn-C_2N is –0.17 eV (Figure S7) with k-point mesh of 2×2×1, which is very close to the value of –0.18 eV with k-point mesh of 3×3×1. Therefore, the k-point mesh of 2×2×1 is used in our manuscript. Therefore, the k-point mesh of 2×2×1 is used in our manuscript.
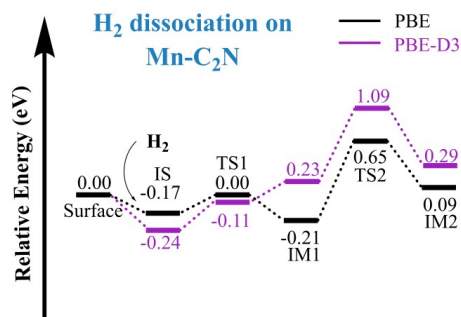

Figure S6. Comparison of the dissociation process of H_2 molecule on Mn-C_2N with PBE and PBE-D3 methods.
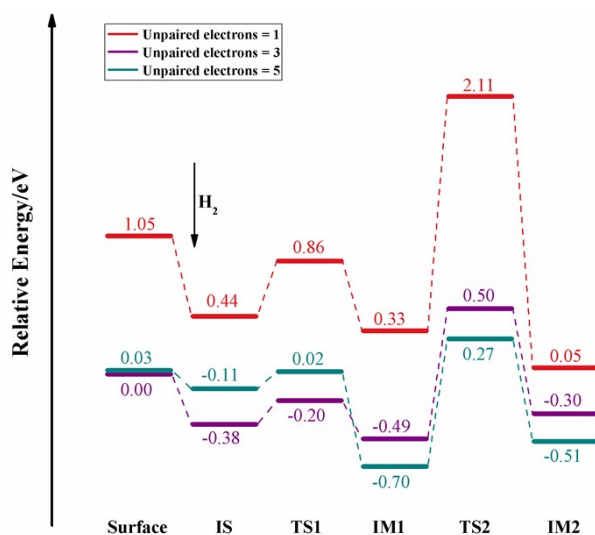

Figure S7. Comparison of the H_2 cleavage on high-spin and low-spin states of Mn-C_2N.

To explore how the spin state of the Mn-C_2N affects the H_2 cleavage, several pathways were computed for the materials with the total magnetic moment set to 1, 3, and 5 μB. As shown in Figure S7, the energy barrier for the H_2 cleavage gradually decreases from 0.42 to 0.18, 0.13 eV for Mn-C_2N with magnetic moment of 1, 3, and 5 μB, respectively, indicating the high-spin state facilitates the cleavage. Also, the H diffusion is easier on high-spin Mn-C_2N, because the diffusion barrier is 0.97, 0.99, and 1.78 eV as the spin moment decreases. It is necessary to note that the optimized total magnetic moment of Mn-C_2N is 4.1 μB, and its total energy is slightly lower than that of Mn-C_2N with magnetic moment of 3 μB by 0.05 eV, suggesting that they are almost

degenerated. This phenomenon is similar to the results reported by Jiang and coworkers very recently[2] that the ORR activity is higher for high-spin state of Fe-C_2N.

References:

1. Zhang, X.; Chen, A.; Zhang, Z. H.; Zhou, Z. Double-Atom Catalysts: Transition Metal Dimer-Anchored C_2N Monolayers as N_2 Fixation Electrocatalysts. *J. Mater. Chem. A*, 2018, **6**, 18599-18604.

2. Zhong, W. H.; Qiu, Y.; Shen, H. J.; Wang, X. J.; Yuan, J. Y.; Jia, C. Y.; Bi, S. W.; Jiang, J. Electronic Spin Moment As a Catalytic Descriptor for Fe Single-Atom Catalysts Supported on C_2N. *J. Am. Chem. Soc.*, 2021, **143**, 4405-4413.